Molecular Crystals and Liquid Crystals

Publication details, including instructions for authors and subscription information:
http://www.tandfonline.com/loi/gmcl20

Anisotropic Weak Localization of Light: From Isotropic Scattering to Ordered Nematic Liquid Crystals

Riccardo Sapienza [a b], Diederik S. Wiersma [c] & Dominique Delande [d]

[a] European Laboratory for Nonlinear Spectroscopy & INFM, Florence, Italy

[b] Laboratoire Kastler-Brossel, Paris, France

[c] European Laboratory for Nonlinear Spectroscopy & INFM, Florence, Italy

[d] Laboratoire Kastler-Brossel, Paris, France

Version of record first published: 31 Aug 2006

To cite this article: Riccardo Sapienza, Diederik S. Wiersma & Dominique Delande (2005): Anisotropic Weak Localization of Light: From Isotropic Scattering to Ordered Nematic Liquid Crystals, Molecular Crystals and Liquid Crystals, 429:1, 193-212

To link to this article: http://dx.doi.org/10.1080/15421400590930935

Mol. Cryst. Liq. Cryst., Vol. 429, pp. 193–212, 2005

ISSN: 1542-1406 print/1563-5287 online
DOI: 10.1080/15421400590930935

Taylor & Francis
Taylor & Francis Group

Anisotropic Weak Localization of Light: From Isotropic Scattering to Ordered Nematic Liquid Crystals

Riccardo Sapienza
European Laboratory for Nonlinear Spectroscopy & INFM, Florence, Italy
Laboratoire Kastler-Brossel, Paris, France

Diederik S. Wiersma
European Laboratory for Nonlinear Spectroscopy & INFM, Florence, Italy

Dominique Delande
Laboratoire Kastler-Brossel, Paris, France

We have performed Monte Carlo simulations of coherent backscattering of vectorial waves in anisotropic Rayleigh media as a preliminary model to approach light scattering in ordered nematic liquid crystals. The cone is anisotropic, consistent with experimental observations and has a shape that is consistent with theory. The role of the penetration length in anisotropic media is discussed.

INTRODUCTION

The transport of light in complex dielectric materials is a rich and fascinating topic of research. Light undergoes multiple scattering when it propagates through inhomogeneous media over distances much larger than one scattering mean free path ℓ_s. Interference can survive random multiple scattering which goes beyond a classical

Dated: August 30, 2004.
We thank B. van Tiggelen for fruitful discussions, INFM (Project RANDS and Photonics), MIURCofin 2002, and Laboratoire Kastler-Brossel de l'École Normale Supérieure et de l'Université Pierre et Marie Curie, UMR 8552 du CNRS. RS acknowledges support from European Community, Marie Curie Fellowship Contract nr HPMT-CT-2000-00102 and the Fondazione Ing. Aldo Gini.
Address correspondence to Riccardo Sapienza, European Laboaratory for Nonlinear Spectroscopy & INFM, Sesto Fiorentino, Florence 50019, Italy. E-mail: sapienza@lens.unipi.it

diffuse transport picture. The most robust example is coherent backscattering or weak localization [1], which manifests itself as an enhancement of the backscattered intensity by a factor of two and a backscattering cone of opening angle λ/ℓ^*, with ℓ^* the transport mean free path, defined as the distance over which the light waves loose memory of propagation direction. Even more dramatic is Anderson localization of light [2], an interference phenomenon that can bring light transport to a halt and therefore change the simple diffusive picture even more.

Liquid crystals in the nematic phase are strongly scattering materials that differ fundamentally from common isotropic random media. The nematic phase of a liquid crystal is characterized by a global alignment of the molecules in a direction called the nematic director **n(r)**, and an otherwise translational disorder. The strong opacity of the nematic phase comes about from local fluctuations in the nematic director $\mathbf{n}(\mathbf{r},\ t) = \mathbf{n}_0 + \delta\mathbf{n}(\mathbf{r},\ t)$, that elastically scatter light [3]. Transmission experiments have shown that light transport in ordered nematic liquid crystals indeed shows anisotropic features, both in static [4] and dynamic [5] experiments, and that diffusive models and radiative transfer theory can describe light transport in such a complex medium [6].

Pioneering experiments on coherent backscattering from nematics have been performed, but only the existence of the interference phenomenon could be confirmed and no other information could be extracted from the experimental data [7]. Anisotropy in coherent backscattering due to an anisotropic transport mean free path has been predicted numerically in Monte-Carlo simulations [8]. Only recently, anisotropy in weak localization from ordered nematic liquid crystals has been observed and the cone fully resolved [9], opening the way for further investigation on light transport in such a complex medium.

No universal recipe exists to generalize a diffusive model for the case of anisotropic scattering. That is, it is not evident how to perform the passage from an anisotropic single-scattering process to anisotropic multiple scattering and subsequently to anisotropic diffusion. A diffusive model is limited by the fact that all characteristics of the transport process have to be contained in one single parameter: the diffusion constant. Single scattering is described by a scattering cross section that depends on incoming and outgoing wavevectors and polarization vectors and can therefore contain various types of anisotropy. The chance of being scattered can depend on propagation direction and polarization, but also the distribution of the light after scattering can be highly anisotropic. In addition, the propagation velocity of the light during the multiple scattering process can be anisotropic as well. A diffusive

model in which all these anisotropies have to be contained in one single parameter is potentially an over-simplification of the problem. In addition, the effect of anisotropy on the boundary conditions, required to solve the diffusion equation, is unknown but of crucial importance.

Ordered nematic liquid crystals are anisotropic scattering media in which light polarization plays a central role: the average medium is birefringent and scattering selection rules favor polarization to flip at each scattering event. Moreover the scattering cross-section and scattering mean free path depend strongly on the polarization state and scattering direction [10]. These intricate scattering properties would suggest that a complete solution of the transport equation is more appropriate than a diffusive model. Unfortunately the coupled hydrodynamics equations of nematic liquid crystals and of the electromagnetic field are very difficult to solve [11]. Our choice is to implement the random walk model in a Monte-Carlo simulation for vectorial waves, in order to calculate numerically light transport in anisotropic media and nematic liquid crystal.

This paper is a first step in the direction of understanding the role of anisotropy in a diffusive and multiple scattering model. The first results of a vectorial Monte Carlo simulation of coherent backscattering and light transport in complex anisotropic systems will be shown.

MULTIPLE SCATTERING

Backscattered Light

In contrast to the case of transmission, backscattered light contains contributions from all path lengths, and thus from all scattering orders. Indeed the main contribution in backscattering comes from single scattering ($\sim$16.8% for isotropic Rayleigh scattering and semi-infinite geometry), and double scattering ($\sim$10.0% for isotropic Rayleigh scattering and semi-infinite geometry) and then all other scattering orders. Thus the backscattered light pattern is very sensitive to the non-isotropic aspects of the lower scattering orders [12], in addition to the anisotropy that survives after averaging over all path lengths.

This is why it is interesting to study how light is backscattered from an anisotropic medium and to use coherent backscattering to probe the system beyond the limits of conventional diffusion theory at all scattering orders. Very accurate coherent backscattering measurements allow to measure very narrow cones from media with transport mean free paths larger than one millimeter [9], opening up the

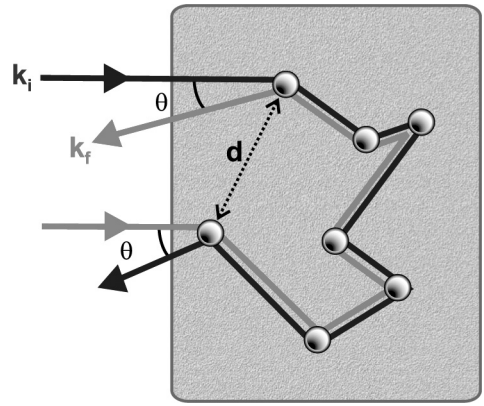

FIGURE 1 Counter-propagating light paths that give rise to coherent backscattering. (See COLOR PLATE XVI)

possibility to perform weak localization studies on nematic liquid crystals, complex fluids and biological tissues, inaccessible to previous coherent backscattering instruments. Monte Carlo simulations of weak localization can be performed with great accuracy and accounting for scattering anisotropy, medium geometry, birefringence, etc...

Coherent backscattering is the result of many two-waves interference patterns

$$I(\theta,\ \phi) = I_0\,(1 + \alpha\,\cos(\mathbf{d}\cdot\Delta\mathbf{k})) \tag{1}$$

where I_0 is the total intensity forgetting interferences, α the contrast of the interference, and we assume no additional phase difference along the reverse paths exists. This interference is generated by counter-propagating light paths with entering-exiting distance $\mathbf{d} = \mathbf{r}_1 - \mathbf{r}_2$ and initial and final k-vectors $\mathbf{k}_i$, $\mathbf{k}_f$, such that $\Delta\mathbf{k} = \mathbf{k}_f + \mathbf{k}_i$ (see Fig. 1). Maximum interference is obtained when the counter-propagating paths have the same amplitude and thus $\alpha = 1$, and only at $\theta = 0$, (see Fig. 2). Here onwards we will assume $\alpha = 1$. The cone is the Fourier transform of the spatial distribution of the intensity of the scattered light on the sample surface, when the latter is illuminated by a point-like source [13]. The triangular top of the coherent backscattered profile is sensitive to the long and diffusive paths and has an opening angle $\Delta\theta \sim \lambda/\ell^*$. The wings, on the other hand, are dominated by the lower spatial frequencies, and therefore by the short paths due to low order scattering. This also means that the top and full width half maximum (FWHM) are determined by the transport mean free path ℓ^*, which is an averaged quantity, whereas the wings are

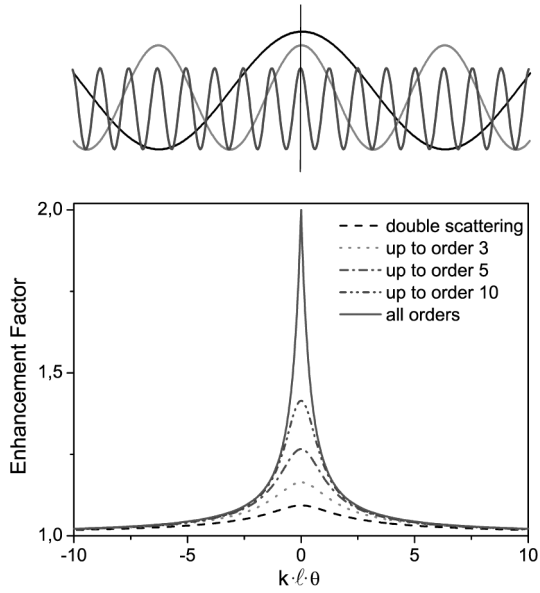

FIGURE 2 Coherent backscattering arises from many two-wave interference patterns which are all in phase at $\theta = 0$. In the figure, the full profile (full line) and the interference that results from only double scattering (dashed line), and a few lower scattering orders (dotted and mixed lines) are shown. The line profile is obtained with a Monte Carlo simulation for scalar waves (single scattering has been subtracted). In the top panel, a few two-paths interference patterns are shown before averaging. (See COLOR PLATE XVII)

strongly influenced by the details of the single scattering differential cross section.

Experimental Measurements of Coherent Backscattering

We have investigated [9] liquid crystal samples consisting of *p*-penthyl-*p*′-cyanobiphenyl (5CB), which were contained in a cylindrical cell of 8 cm diameter and 4 cm thickness, which satisfies the requirement of having an optically thick sample. The setup is shown in Figure 3. An angular resolution of 10 μrad was obtained, two orders of magnitude higher than previous liquid crystal work, and ∼10 times better than the highest resolution reported in the literature.

We report the coherent backscattering cone as recorded in long linear scans in the two orthogonal scanning directions, after precise determination of the exact backscattering angle. The light is incident normal to the front sample interface, and the magnetic field lays in the

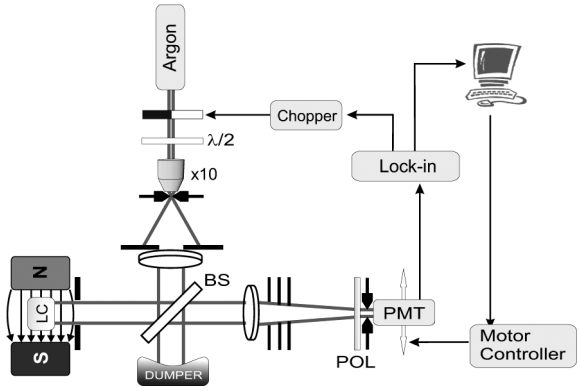

FIGURE 3 Sketch of the setup for the coherent backscattering measurement. A diffraction limited 8 cm diameter collimated laser beam is obtained by expanding and spatially filtering the output of a single mode Argon laser (2W, 488 nm). This beam is reflected from a 15 cm wide beam splitter (BS) onto the sample (LC) which is placed between the poles of an electro-magnet. The backscattered light from the sample is collected through the beam splitter by a wide achromatic triplet lens (f = 1250 mm) and monitored by a photomultiplier tube (PMT) through a polarizer (POL) and a 10 μm diameter pinhole placed exactly in the focal plane of the achromatic lens. All lenses are aligned perpendicular to the optical beams to avoid astigmatism, and the response of the setup is carefully checked to be isotropic. (See COLOR PLATE XVIII)

plane orthogonal to $\mathbf{k}_i$. An external magnetic (or electric) field can induce a global alignment of the crystals, which find energetically convenient to be parallel to the field (Fig. 4). We can observe that the coherent backscattering cone in the scattering plane parallel to the nematic director is narrower than the cone in the perpendicular plane. Note that the observed anisotropy cannot be due to polarization effects at the sample surface (like e.g. birefringent internal reflection [14]) since we are comparing angular scans with the same polarization direction. The solid line in Figure 5 was obtained from a simple coherent backscattering model generalized for an anisotropic system, and based on the diffusion approximation even if no actual justification of the validity of this model can be given at this point. The rounded top is due to the finite experimental resolution.

A two-dimensional fit of the measured coherent backscattering data can be used to extract values for the transport mean free paths. Doing this we have assumed that upon multiple scattering a diffusive transport mean free path can be defined which is not any more a scalar quantity, but a vectorial one. We denote its components parallel and

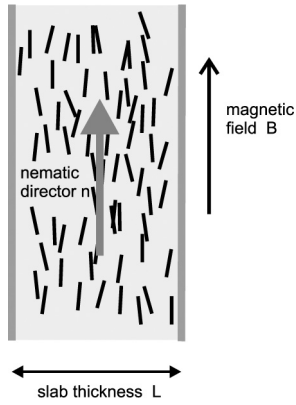

FIGURE 4 An external magnetic field can induce a global alignment of the nematic liquid crystals around a common direction **n** called the nematic director, parallel to the magnetic field **B**.

perpendicular to **n** by $\ell_{\parallel}^{*}$ and $\ell_{\perp}^{*}$ respectively [9,15]. The only fitting parameters are the enhancement factor and the values of $\ell_{\parallel}^{*}$ and $\ell_{\perp}^{*}$. For the extraordinary polarization case we find mean free paths $\ell_{\parallel}^{*} = 0.71\,\text{mm}$ and $\ell_{\perp}^{*} = 0.83\,\text{mm}$, with a fitting error of about 2.5% and a statistical error of 4%. The fitting error refers to the uncertainty in the values of the fitting parameters for each measurement, while the statistical one is related to the spreading of these values

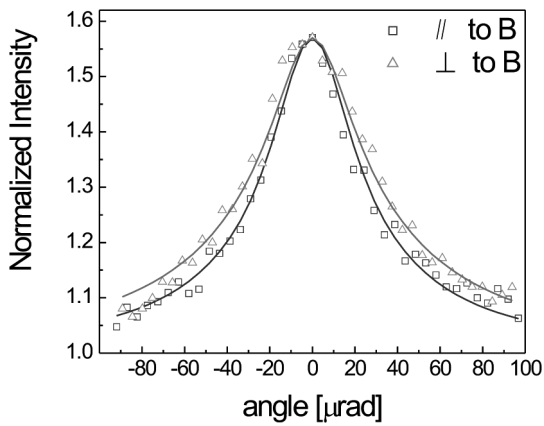

FIGURE 5 Coherent backscattering cone from a monodomain nematic for both orthogonal scanning directions, in a linear plot. The nematic director and polarization vector are in the same direction, parallel to **B**. (See COLOR PLATE XIX)

when repeated measurements are performed. The resulting anisotropy is: 1.17 ± 0.04. For the other case, ordinary polarization, we find: $\ell^*_{\parallel} = 0.67\,\text{mm}$ and $\ell^*_{\perp} = 0.77\,\text{mm}$, and $\ell^*_{\parallel}/\ell^*_{\perp} = 1.15 \pm 0.04$. The isotropic case, when no orientation around a common director can be defined, gives: $\ell^*_{\parallel}/\ell^*_{\perp} = 1.01 \pm 0.04$. These anisotropy values are in good agreement with available theories regarding anisotropic diffusion in nematics [6] that predict a mean free path anisotropy of about 1.18.

FROM SINGLE TO MULTIPLE SCATTERING

Anisotropy affects both the single scattering properties and the average medium in which the light propagates. The passage from single to multiple scattering requires therefore the definition of $G(\mathbf{k}, \mathbf{r}_{12})$, the amplitude Green function of the system, which describes how the light amplitude propagates between two scattering events. Whereas for isotropic scattering one usually employs a direction independent propagator

$$G(\mathbf{k}, \mathbf{r}_{12}) = -\frac{1}{4\pi r_{12}} \exp(ikr_{12}) \exp\left(-\frac{r_{12}}{2\ell_s}\right), \tag{2}$$

in anisotropic media one often cannot neglect the birefringence and the direction dependence of the scattering mean free path $\ell_s(\Omega_i)$. The Green function in Eq. 2 is simply a spherical wave $\exp(ikr_{12})/4\pi r_{12}$ attenuated by the Beer-Lambert factor $\exp(-r_{12}/2\ell_s)$ which takes into account the presence of the scattering medium; $\mathbf{k}$ is the wave vector inside the medium, with real and imaginary part.

Optical birefringence in ordered nematics is present as rotational symmetry is broken by the nematic director $\mathbf{n}$. Light propagates through nematic liquid crystals in two characteristics modes. These are the *ordinary* mode $|\mathbf{k}, \mathbf{o}\rangle$, which has polarization $\mathbf{o}$ orthogonal to $\mathbf{n}$ and $\mathbf{k}$ and the *extraordinary* one $|\mathbf{k}, \mathbf{e}\rangle$ whose polarization $\mathbf{e}$ is in the plane of $\mathbf{k}$ and $\mathbf{n}$. The ordinary mode behaves as in an isotropic system, while the extraordinary mode possesses a direction-dependent index of refraction and its phase and group velocities are not equal and parallel. Birefringence lifts the polarization degeneracy of the propagating modes which become distinct (see Fig. 6). The two eigenstates experience a different refractive index $n_o \neq n_e$, and therefore interference between them can be neglected after a distance $\Delta r \simeq \lambda/(n_o - n_e)$. For nematics, $\Delta r \simeq 2 - 3\,\mu\text{m}$, which is much smaller than the length scales of the scattering process, $\Delta r << \ell_s \simeq 50 - 100\,\mu\text{m}$ [10]. For this reason the two eigenstates can be treated independently.

For isotropic systems, the scattering mean free path ℓ_s is usually defined as the average distance between two scattering events, and

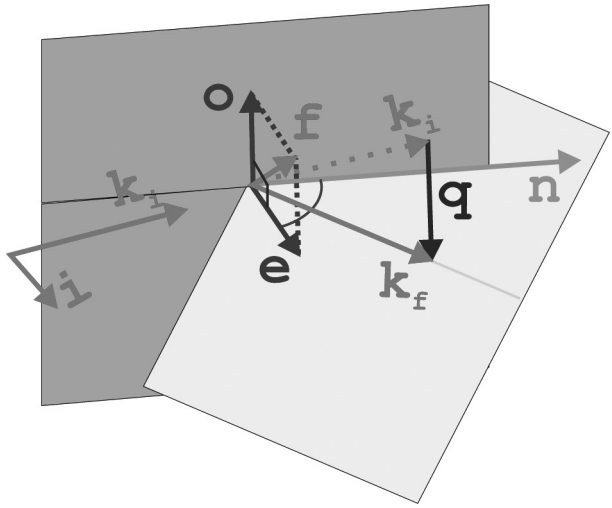

FIGURE 6 Scattering geometry: the photon state $|\mathbf{k}_i, \mathbf{i}\rangle$ is scattered into $|\mathbf{k}_f, \mathbf{f}\rangle$. The nematic director $\mathbf{n}$ and the transferred momentum $\mathbf{q} = \mathbf{k}_f - \mathbf{k}_i$ are shown. $\mathbf{k}_f, \mathbf{n}$ and $\mathbf{e}$ are in the same plane, orthogonal to the plane defined by $\mathbf{n}$ and $\mathbf{o}$. The polarization can be decomposed into the two propagation eigenmodes $\mathbf{o}$ and $\mathbf{e}$. Ω_i and Ω_f, which indicate the directions of $\mathbf{k}_i$ and $\mathbf{k}_f$, are not shown here. (See COLOR PLATE XX)

is inversely proportional to the scattering cross section:

$$\ell_s = \frac{1}{\rho\sigma_t} = \left[\rho \int \frac{d\sigma}{d\Omega}\, d\Omega\right]^{-1}, \tag{3}$$

where ρ is the spatial density of the scatterers. In nematics, the scattering mean free path ℓ_s will depend also on the incident direction Ω_i

$$\ell_s(\Omega_i) = \left[\frac{1}{V}\int \frac{d^2\sigma}{d\Omega_i d\Omega_f}\, d\Omega_f\right]^{-1}. \tag{4}$$

The propagator $G(|\mathbf{k}, \mathbf{e}/\mathbf{o}\rangle, \mathbf{r_{12}})$ of each of the eigenmodes of the medium is related to the scattering mean free path $\ell_s(|\mathbf{k}, \mathbf{e}/\mathbf{o}\rangle)$. The Beer-Lambert's law that determines the exponential attenuation of the wave intensity reads:

$$I(\mathbf{r}, |\mathbf{k}, \mathbf{e}/\mathbf{o}\rangle) = I(\mathbf{r}_0, |\mathbf{k}, \mathbf{e}/\mathbf{o}\rangle) \exp\left(-\frac{|\mathbf{r} - \mathbf{r}_0|}{\ell_s(|\mathbf{k}, \mathbf{e}/\mathbf{o}\rangle)}\right). \tag{5}$$

If one tries to identify a dominant transport direction, one is tempted to look at the scattered k-vectors which correspond to maxima

of the radiated pattern $d^2\sigma/d\Omega_i d\Omega_f$. In a birefringent anisotropic system this can be inaccurate however: a local maximum in the differential cross-section for a given direction is not directly a local peak in the photon density. In a direction of the scattered wavevector in which $d^2\sigma/d\Omega_i d\Omega_f$ is large, $\sigma_t(\Omega_i) = \int (d^2\sigma/d\Omega_i d\Omega_f) d\Omega_f$ can be large as well, so that the scattering mean free path is short. Many photons are radiated in such a direction, but they suffer from intense scattering into all angles which depletes the light flow.

We stress here that light transport quantities can be properly defined only after ensemble averaging of the above picture. This averaging can be done in a numerical but exact way with Monte Carlo simulations.

MONTE CARLO SIMULATION

A random walk model can be well implemented in a Monte Carlo simulation which can take into account all features of the scattering event and of the successive propagation. The principle of a Monte Carlo simulation is to probe the system in a large number of configurations, and to use the result to describe the whole system [16]. If the static single scattering cross-section $d^2\sigma/d\Omega_i d\Omega_f$ and the propagator $G(|\mathbf{k}, \mathbf{e}/\mathbf{o}\rangle, \mathbf{r}_{12})$ are known, then the Monte Carlo simulation will just perform the configuration averaging. Many light wavepackets, which we will call for simplicity photons, but which are of classical nature, are launched into the system and properly propagated; the exiting intensity is then recorded. The model can be effectively used to probe the transport properties of the systems exactly, but great care has to be taken to model the nematic liquid crystal. The scattering event is ruled by the single scattering cross-section (see Eq. 6), which depends on the input and output state and in particular on the orientation of the polarization and propagation vectors with respect to the nematic director [3]

$$\frac{d^2\sigma}{d\Omega_i d\Omega_f} = V\left(\frac{\Delta\varepsilon k^2}{4\pi}\right)^2 \sum_{\alpha=x,y} \frac{k_b T (i_x f_z + i_z f_\alpha)^2}{K_\alpha q_\perp^2 + K_3 q_\parallel^2 + K_1 \xi^{-2}}, \tag{6}$$

(here we follow the formalism defined in De Gennes's book [3] depicted in Fig. 6). K_i are the Frank elastic constants, and $\mathbf{q} = \mathbf{k}_f - \mathbf{k}_i$ the scattering wave vector; the polarization product $i_x f_z + i_z f_\alpha$ determines the polarization selection rules while the denominator is dominated by $K_1 \xi^{-2}$ which depends on the external magnetic field. The dependence on q^{-2} accounts for the strong directionality of the cross-section, whose divergence for $|\mathbf{q}| \longrightarrow 0$ is prevented by a finite value of ξ. The prefactors in Eq. 6 are the temperature T, the Boltzman constant k_b, the modulus of the light k-vector k, the anisotropy in the dielectric constant

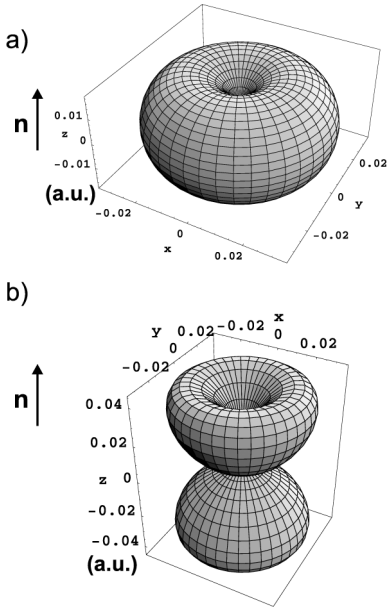

FIGURE 7 Total integrated cross-section σ_t for light scattering in nematic liquid crystals: panel a) an extraordinary mode into an ordinary (or ordinary into extraordinary); panel b) an extraordinary mode into an extraordinary. One can see that σ_t, the total probability for a photon of being scattered, depends on the direction of propagation and on the polarization state. Nematic director in the z-direction for all cases. 5CB liquid crystals in a magnetic field of $0.5\,\mathrm{T}$, $K_3 = 5.3 \times 10^{-12}\,\mathrm{J}$, $K_1 = 0.79\,K_3$ and $K_2 = 0.43\,K_3$, $\xi = 4.2\,\mu\mathrm{m}$. (See COLOR PLATE XXI)

$\Delta\varepsilon = \varepsilon_{\|} - \varepsilon_{\perp}$ and the scattering volume V. At a wavelength of 405 nm $\Delta\varepsilon = 0.81168$.

Figure 7 shows the anisotropy of the total scattering cross-section σ_t for different polarization eigenmodes of the input and output polarization, as a function of the scattered k-vector. In the case of scattering of an extraordinary mode into an ordinary, the total scattering cross-section is extremely small for k-vectors in the direction of the nematic director (panel a), while for the extraordinary-extraordinary case also the plane orthogonal to **n** exhibits a minimum value of σ_t (panel b).

The process of double scattering is depicted in Figure 8 for the case of ordinary light incident with k-vector parallel to **n**, scattered into extraordinary light and then double-scattered into ordinary light after an average distance ℓ_s. The emerging light distribution is calculated with a second scattering cross-section.

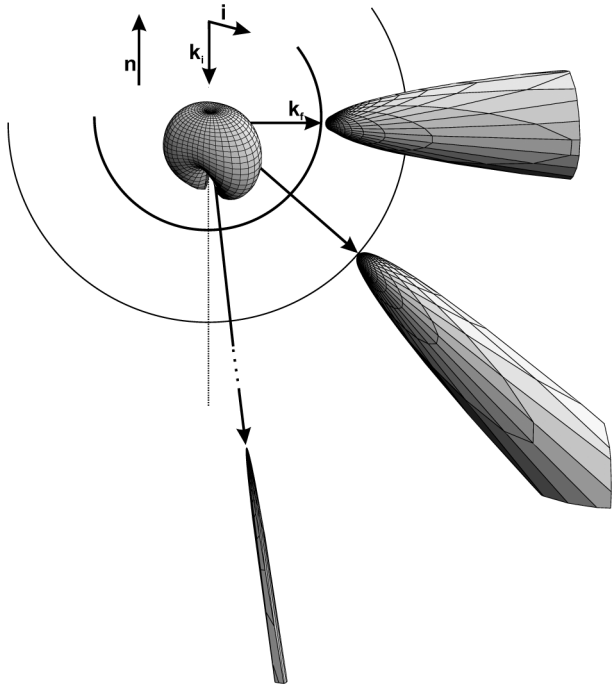

FIGURE 8 Double scattering process in ordered nematic liquid crystals. Ordinary light incident with k-vector parallel to **n** is scattered into extraordinary light with a differential cross-section shown in the center of the picture. Three possible directions are shown. Light propagates for an average distance given by ℓ_s, shown by the length of the arrows, before the second scattering event. The second scattering cross-section is plotted for the case in which the emerging light is ordinary. The top most scattering event occurs at a distance extremely long and is very rare. (See COLOR PLATE XXII)

We can see that already for the simplest process of two events of scattering, both of the two light eigenmodes are involved, ordinary and extraordinary, and that their scattering cross-sections are very different.

In view of these features, in the Monte Carlo simulation any scattered photon has to be projected onto the birefringent eigenmodes which then can be propagated ballistically. Their direction of propagation follows the photon group velocity in the nematic average medium and the travelled distance before the following scattering event is governed by an anisotropic Lambert-Beer's probability (see Eq. 5) which itself depends on the photon state: it is an anisotropic random walk. When the photon exits the medium, the interference

contribution of its path and its reverse counterpart are calculated from Eq. 1. The coherent backscattering cone is obtained by the sum of all this interference patterns.

Our strategy is based on an approach with increasing complexity. We start with a model of isotropic Rayleigh scattering. Then we extend it to include scattering and spatial anisotropy, at first keeping the intra-scattering medium homogeneous and isotropic and then with the anisotropic propagation eigenmodes. As a last stage light scattering in ordered nematics can be modelled without ambiguity. Here we present the results obtained if angular anisotropy is introduced into the Rayleigh scattering process.

Isotropic Rayleigh Scattering

If the size of the scattering centers is smaller than the radiation wavelength, then the scattering can be described by an induced linear electronic dipole, which is excited by the incident light and which radiates. This is one of the most common scattering process. Usually the strength of this dipole is directly proportional to the incident light polarization. The probability of a scattering event in a certain direction is then given by the projection of the excited dipole into the output polarization state,

$$\frac{d\sigma}{d\Omega}(\mathbf{k}_f) = \frac{3\sigma_0}{8\pi}(1 - |\mathbf{i} \cdot \mathbf{k}_f|^2). \tag{7}$$

In this case the scattering mean free path is also isotropic, as the total cross section is a scalar which doesn't depend on the scattered direction $\mathbf{k}_f$:

$$\sigma_t = \int \frac{d\sigma}{d\Omega}(\mathbf{k}_f)\, d\Omega = \sigma_0. \tag{8}$$

For any incident light state, the Rayleigh scattering cross-section has always the same shape, just rotated accordingly to the incident polarization; the scattering mean free path is a scalar constant of the medium. This means that upon ensemble averaging, no favorite direction can emerge, and the overall scattering process becomes completely isotropic after a few events.

Anisotropic Rayleigh Scattering

We can generalize this isotropic picture and allow for a non-isotropic polarizability of the medium, ex. asymmetric molecules that can be

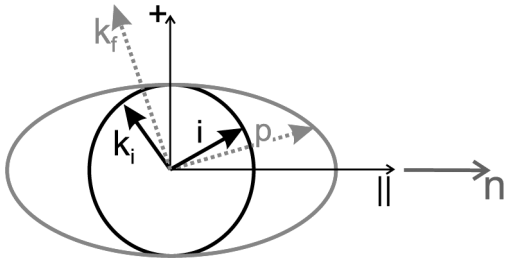

FIGURE 9 Effect of the anisotropy on the excited dipole $\mathbf{p} = \mathbf{D}\mathbf{i}$. The diploe is stronger and rotated towards $\mathbf{n}$; therefore the scattering is more probable in the direction orthogonal to $\mathbf{n}$. (See COLOR PLATE XXIII)

more easily excited by a field in a given direction. This common axis will be the same for all dipoles, and will not average out upon multiple scattering: the overall pattern will be anisotropic. We can model the scatterer polarizability with an uniaxial anisotropic dielectric tensor $\mathbf{D} = \mathbf{1} + (a-1)|\mathbf{n}\rangle\langle\mathbf{n}|$,

$$\mathbf{D} = \begin{pmatrix} a & 0 & 0 \\ 0 & 1 & 0 \\ 0 & 0 & 1 \end{pmatrix} \tag{9}$$

where a is the microscopic parameter determining the degree of anisotropy, being $a = \langle\mathbf{n}|\mathbf{D}|\mathbf{n}\rangle$, the value assumed by the dielectric tensor in the direction of the optical axis. The dipole $\mathbf{p}$ induced by the incident polarization $\mathbf{i}$ is then

$$\mathbf{p}(\mathbf{i}) = \mathbf{D}\mathbf{i} = (a-1)(\mathbf{i}\cdot\mathbf{n})\mathbf{n} + \mathbf{i}. \tag{10}$$

If $a \neq 1$, the dipole is not unitary, being $|\mathbf{p}|^2 = (a^2-1)(\mathbf{i}\cdot\mathbf{n})^2 + 1$, and it is rotated towards $\mathbf{n}$: light emission is more probable for those scattered k-vectors in the plane orthogonal to $\mathbf{n}$, Figure 9. On the other hand, each state experiences a different σ_t

$$\sigma_t(\mathbf{f}) = \sigma_0[(\mathbf{f}\cdot\mathbf{n})^2(a^2-1) + 1], \tag{11}$$

and therefore has a different probability of being scattered. This turns into a scattering mean free path $\ell_s = 1/\rho\sigma_t$ that is not isotropic and in particular a^2 times smaller for k-vectors in the direction perpendicular to $\mathbf{n}$ (and polarization parallel to $\mathbf{n}$)

$$\ell_{s\perp} \sim \frac{\ell_{s\parallel}}{a^2}. \tag{12}$$

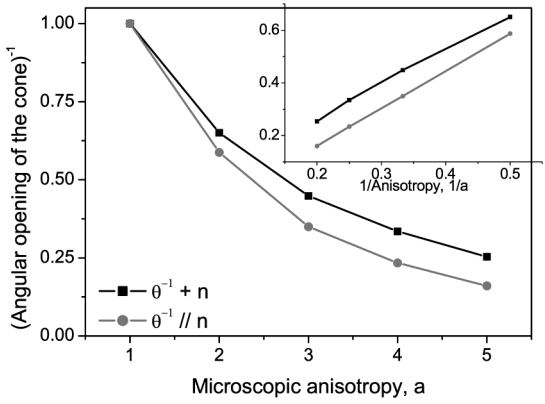

FIGURE 10 Reciprocal of the angular opening of the cone as a function of the anisotropy a, for incident extraordinary polarization, $\mathbf{i} \parallel \mathbf{n}$, 100 000 photons launched, optical thickness $b = 100$. In first approximation the behavior of $\theta^{-1}_{\perp,\parallel}$ (a) is hyperbolic. It is important to notice the anisotropy that opens up between the two angles. (See COLOR PLATE XXIV)

In the simulations light is incident normal to the slab, and the optical axis **n** lies in the plane of the slab surface. We have performed two different simulations, for the two input polarization state of the light, parallel and perpendicular to **n**. In both cases we have used the isotropic propagator, generalized for an anisotropic scattering mean free path, neglecting the anisotropy-induced birefringence.

The top of the backscattering cone is determined by the transport mean free path. In the isotropic case the relation between ℓ^* and the angular opening $\Delta\theta$ is: $\ell^* \sim (0.7/2\pi)\,\lambda/\Delta\theta$. The angular opening of the cone is extracted from linear fits of the triangular top of the cone. Two angles are obtained, $\theta_\parallel$ and $\theta_\perp$, in the direction parallel and perpendicular, respectively, to the nematic director. In Figure 10 we show how, in the case of extraordinary polarization, the reciprocal of the angular opening of the cone evolves as a function of the single scattering anisotropy a. It decreases hyperbolically, as seen from the inset. We can perform the same analysis for the ordinary incident polarization (Fig. 11) and find a similar behavior.

The backscattered light profile is crucially determined by the penetration length z_p of the photon in the medium, before the first scattering event, see Figure 12. In the anisotropic medium two different penetration lengths are important, for input polarization parallel or perpendicular to **n**. A different z_p implies a different number of

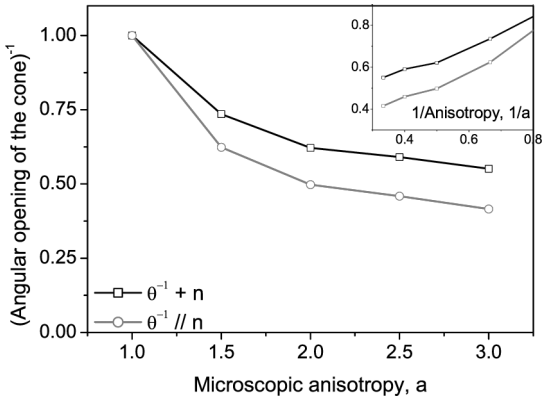

FIGURE 11 Reciprocal of the angular opening of the cones as a function of the anisotropy a, for incident ordinary polarization, $\mathbf{i} \perp \mathbf{n}$, 100 000 photons launched, optical thickness $b = 100$. Again anisotropy opens up between $\theta_{\perp}^{-1}$ and $\theta_{\parallel}^{-1}$. (See COLOR PLATE XXV)

scattering events before exiting the medium, therefore a different mixing of the two mean free path $\ell_{\perp}^{*}$ and $\ell_{\parallel}^{*}$.

A very important quantity is the angular anisotropy $(\theta_{\perp}^{-1} - \theta_{\parallel}^{-1})/\theta_{\perp}^{-1}$, which is plotted in Figure 13 and which increases with a, as qualitatively expected. Also in the isotropic case ($a = 1$) a polarization

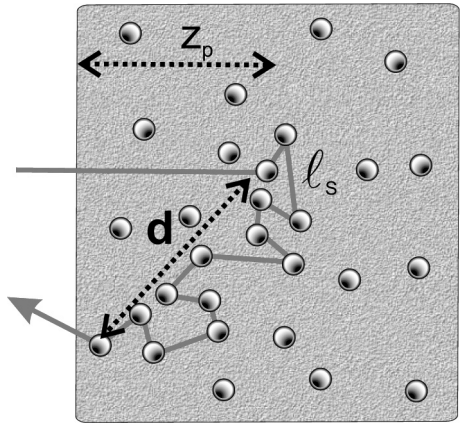

FIGURE 12 Diffusion in backscattering due to anisotropy. The penetration length is z_p while the exiting distance d is obtained from the interplay of z_p and ℓ_s. (See COLOR PLATE XXVI)

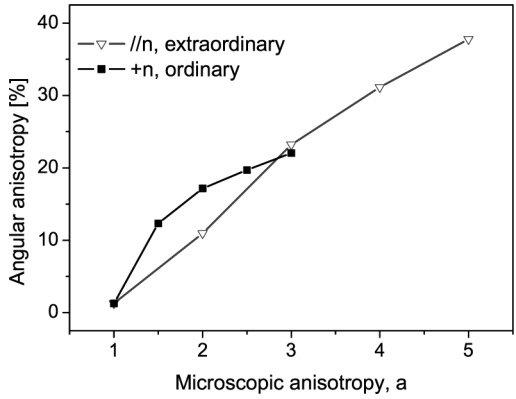

FIGURE 13 Anisotropy of the reciprocal of the angular opening of the cone, $(\theta_{\perp}^{-1} - \theta_{\parallel}^{-1})/\theta_{\perp}^{-1}$, as a function of the microscopic anisotropy a, for $\mathbf{i} \parallel \mathbf{n}$ extraordinary incident polarization (empty triangles) and $\mathbf{i} \perp \mathbf{n}$ ordinary incident polarization, (full squares). 100 000 photons launched, optical thickness $b = 100$. The lines are a guide to the eyes.

anisotropy is present in the wings of the cone, but not in the angular opening of its top. This effect is known and related to the first scattering orders which show polarization anisotropy (see ref. [1]) which is not related to the microscopic anisotropy a.

Figure 14 shows the simulated cones for extraordinary polarization, parallel to **n**. The penetration length in this case is very short, $z_p = \ell_s/a^2$, a^2 times smaller than the isotropic scattering mean free path. Therefore few events are enough for the photon to escape the medium. The exiting distance vector **d** of the photons is thus dominated by low scattering orders, which have strong signature of the single scattering anisotropy. This reflects into the large anisotropy of the cone wings.

Figure 15 shows the case of ordinary incident polarization. The penetration length is long, $z_p = \ell_s$, equal to the isotropic scattering mean free path and therefore a photon has to perform many more scattering events before exiting the medium (see Fig. 12). The transport will be dominated by the averaged transport mean free path. Again the wings are a clear indication of an averaging process that reduces the effect of single scattering anisotropy: both the parallel and perpendicular cuts show a large angle behavior similar to the isotropic case, which is clearly different from the case reported in Fig. 14. On the contrary, if one looks at the diffusive top, and one extracts the information about the opening angle, one sees a clear anisotropy between $\theta_{\perp}^{-1}$ and $\theta_{\parallel}^{-1}$ which increases with the parameter a (Fig. 13}, filled squares).

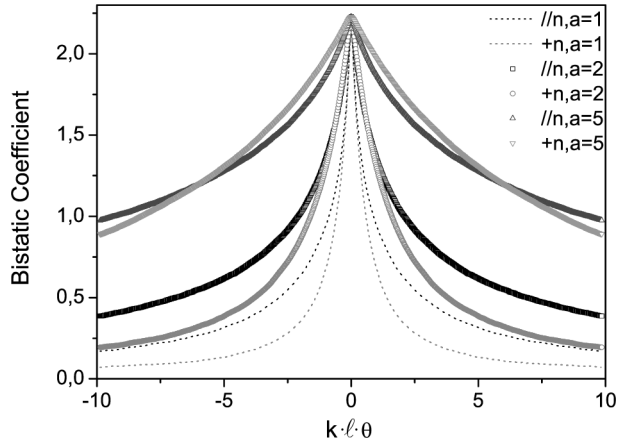

FIGURE 14 Comparison of the coherent backscattering cone for isotropic scattering (dotted line) and the cone in presence of angular anisotropy. Extraordinary input polarization, $\mathbf{i} \parallel \mathbf{n}$, short penetration length. Plots as a function of anisotropy a, for optical thickness $b = 30$, and 100 000 photons launched. Anisotropic bistatic coefficients are rescaled to be compared with the isotropic one. (See COLOR PLATE XXVII)

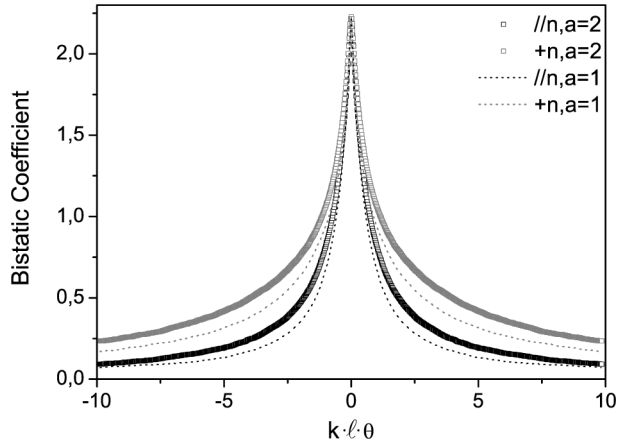

FIGURE 15 Comparison of the coherent backscattering cone for isotropic scattering (dotted line) and the cone in presence of angular anisotropy. Ordinary input polarization $\mathbf{i} \perp \mathbf{n}$, long penetration length. Optical thickness $b = 30$, and 100 000 photons launched. Anisotropic bistatic coefficients are rescaled to be compared with the isotropic one. (See COLOR PLATE XXVIII)

CONCLUSIONS

We have observed angular anisotropy in weak localization of light from highly scattering, orientationally ordered, nematic liquid crystals. No exact theory is available at this moment to describe the phenomenon. To approach it with a simpler and clearer model we have performed Monte Carlo simulations of vectorial waves propagating in anisotropic Rayleigh scattering media, with isotropic propagator and anisotropic scattering mean free path. We obtain anisotropic coherent backscattering cones as a function of the microscopic parameter a that rules the anisotropy of the single-scattering cross-section. The cone profile can be described well with a diffusive model only as far as the top is concerned. The wings show a more complex behavior, which is a consequence of the sensitivity of the penetration length on the incident light state. As further investigation the Monte Carlo simulation will be extended to include also birefringent light propagation in ordered nematic liquid crystals, and the nematic single scattering cross-section.

REFERENCES

[1] Kuga, Y. & Ishimaru, A. (1984). *J. Opt. Soc. Am. A*, *8*, 831; van Albada, M. P. & Lagendijk, A. (1985). *Phys. Rev. Lett.*, *55*, 2692; Wolf, P. E. & Maret, G. (1985). *Phys. Rev. Lett*. *55*, 2696.

[2] John, S. (1984). *Phys. Rev. Lett.*, *53*, 2169; Anderson, P. W. (1985). *Phil. Mag. B*, *52*, 505.

[3] de Gennes, P. G. & Prost, J. (1993). *The Physics of Liquid Crystals* 2nd edition. Oxford: New York. Chandrasekhar S. *Liquid Crystals* (Cambridge Univ. Press, Cambridge, 1977); Val'kov A. Y. & Romanov, V. P. (1982). Zh. Eksp. Teor. Viz., *82*, 1777. [*Sov. Phys. JETP*, *56*, 1028 (1983)].

[4] Kao, M. H., Jester, K. A., Yodh, A. G., & Collings P. J. (1996). Observation of Light Diffusion and Correlation Transport in Nematic Liquid Crystals. *Phys. Rev. Lett.*, *77*, 2233.

[5] Wiersma, D. S., Muzzi, A., Colocci, M., & Righini, R. (1999). Time-resolved anisotropic multiple light scattering in nematic liquid crystals. *Phys. Rev. Lett.*, *83*, 4321.

[6] Romanov, V. P. & Shalaginov, A. N. (1988). *Opt. Spectrosc.*, *64*, 774. van Tiggelen, B. A., Maynard, R., & Heiderich, A. (1996). *Phys. Rev. Lett*., *77*, 639; Stark H. & Lubensky, T. C. (1996). *Phys. Rev. Lett*., *77*, 2229.

[7] Kuzmin, L. V., Romanov, V. P., & Zubkov, L. A. (1996). *Phys. Rev. E*, *54*, 6798; Vithana, H. K., Asfaw, L., & Johnson, D. L. (1993). *Phys. Rev. Lett*. *70*, 3561.

[8] Heiderich, A., Maynard, R., & van Tiggelen, B. A. (1997). *J. Phys. II*, (France) *7*, 765.

[9] Sapienza, R., Mujumdar, S., Cheung, C., Yodh, A. G., & Wiersma, D. S. (2004). Anisotropic Weak Localization of Light. *Phys. Rev. Lett.*, *92*, 033903.

[10] van Tiggelen, B. A. & Stark, H. (1990). Nematic liquid crystals as a new challenge for radiative transfer. *Rev. Mod. Phys. Cond. Mat.*, *2*, 7653.

[11] Liu, M. (1994). Maxwell equations in nematic liquid crystals. *Phys. Rev. E*, *50*, 2925.
[12] Pine, D. J., Weitz, D. A., Chaikin, P. M., & Herbolzheimer, E. (1988). Diffusing wave spectroscopy. *Phys. Rev. Lett.*, *60*, 1134–1137.
[13] Lenke, R. & Maret, G. (2000). *Eur. Phys. J. B*, *17*, 171.
[14] Lagendijk, A., Vreeker, B., & de Vries, P. (1989). *Phys. Lett. A*, *136*, 81.
[15] Johnson, P. M., Bret, B. P. J., Rivas, J. G., Kelly, J. J., & Lagendijk, A. (2002). Anisotropic Diffusion of Light in a Strongly Scattering Material. *Phys. Rev. Lett.*, *89*, 243901.
[16] Labeyrie, G., Delande, D., Mller, C. A., Miniatura, C., & Kaiser, R. (2003). Coherent backscattering of light by an inhomogeneous cloud of cold atoms. *Phys. Rev. A*, *67*, 033814.